Supporting Information

Solvent and Concentration Effects on Highly Defined, Colloid-Like Ionic Clusters in Solution

*Jana Eisermann, Lukas Prager and Dariush Hinderberger**

Jana Eisermann, Prof. Dr. Dariush Hinderberger
Institute of Chemistry
Martin-Luther-Universität Halle-Wittenberg
Von-Danckelmann-Platz 4, 06120 Halle (Saale), Germany
E-mail: dariush.hinderberger@chemie.uni-halle.de
web: http://www.epr.uni-halle.de/
phone: +49 (0)345 55-25230

Lukas Prager
Landesschule Pforta
Schulstraße 12, 06628 Schulpforte, Germany

Preparing solvent mixtures

The preparation of all the final solvent mixtures, which were used in our study, is based on the simple procedure of combining the pure solvents in the right volume proportions. Table S.1 enumerates the composition of the solvents, which contain different volume stoichiometries of DMSO and glycerol 88 wt% aqueous solution.

Table S.1: Preparation of all solvent mixtures with altering the volume stoichiometry of the 'stock solvents' DMSO and glycerol 88 wt%

volume stoichiometry DMSO:glycerol:water	volume DMSO / ml	volume glycerol 88 wt% / ml
33:57:10	1	2
25:64:11	1	3
20:68:12	0.5	2
10:77:13	0.4	3.6
67:28:5	2	1
75:21:4	3	1
80:17:3	2	0.5
90:9:1	3.6	0.4
100:0:0	1	0
0:85:15	0	1

The stated ratios of DMSO:glycerol:water (v/v/v) were calculated using the density of glycerol 88 wt% ($\rho_{gly88} = 1.226 \frac{g}{cm^3}$) and pure glycerol ($\rho_{gly} = 1.261 \frac{g}{cm^3}$) as well as the respective volume of glycerol 88 wt% (V_{gly88}) from Table S.1. Equation S.1 summarizes the convertion of glycerols weight percentage into his final volume percentage (v_{gly}) for each solvent mixture

$$v_{gly} = \frac{w \, V_{gly88} \, \rho_{gly88}}{\rho_{gly}} \quad \text{with} \quad w = 88 \text{ wt\%.} \tag{S.1}$$

Table S.2 lists the manufactoring for all solvents with a constant amount of DMSO, but gradually changing the glycerol:water ratio. Note that here we used glycerol ≥ 98 wt% aqueous solution to produce the different solvent compositions. Furthermore, the calculation of the final volume percentages for DMSO:glycerol:water was simplified, because we only divided the specific volume from each compound with the total volume of the solvent mixture and neglected the impurity of glycerol ≥ 98 wt% except for the last mixture 40:49:1 (v/v/v).

Table S.2: Preparation of all solvent mixtures with altering the glycerol:water ratio

glycerol:water volume ratio DMSO;glycerol:water	volume DMSO / ml	volume glycerol / ml	volume water / ml
50:5:45	2	0.2	1.8
50:10:40	2	0.4	1.6
50:15:35	2	0.6	1.4
50:20:30	2	0.8	1.2
50:25:25	2	1.0	1.0
50:30:20	2	1.2	0.8
50:35:15	2	1.4	0.6
50:40:10	2	1.6	0.4
50:45:5	2	1.8	0.2
50:49:1	2	2.0	0.0

Preparing bulk concentrations

Decreasing the bulk concetration of $\mathbf{1}^{4+}$:$\mathbf{2}^{2-}$ (respectively $\mathbf{1}^{4+}$:$\mathbf{3}^{2-}$) started with producing following stock solutions in DMSO:glycerol:water 50:43:7 (v/v/v):

- 2 mM $\mathbf{1}^{4+}$ and

- 6 mM $\mathbf{2}^{2-}$ (respectively $\mathbf{3}^{2-}$).

The two stock solutions were then diluted separately into the desired concentrations in Table S.3, which we combined in a 1:1 (v/v) stoichiometry to gain the final concentration ratios.

Table S.3: Concentrations of $\mathbf{1}^{4+}$ and $\mathbf{2}^{2-}$ (respectively $\mathbf{3}^{2-}$) before preparing the final ratios for DLS and CW EPR spectroscopy

concentration ratio / mM:mM	concentration $\mathbf{1}^{4+}$ / mM	concentration $\mathbf{2}^{2-}$ ($\mathbf{3}^{2-}$) / mM
0.5:1.5	1	3
0.2:0.6	0.4	1.2
0.1:0.3	0.2	0.6
0.05:0.15	0.1	0.3
0.02:0.06	0.04	0.12
0.01:0.03	0.02	0.06

A similar setup was used for the ratio of 1.5 mM : 4.5 mM, but we increased the stock solution concentration of $\mathbf{1}^{4+}$ to 3 mM and for $\mathbf{2}^{2-}$ (respectively $\mathbf{3}^{2-}$) to 9 mM.

Dynamic Light Scattering (DLS) measurements

The ALV device with a fixed backscattering angle of $\theta = 173°$ obtains the intensity time correlation function $g_2(\tau)$ from the homodyne detected scattering intensity using an ALV-5000/E multiple tau digital correlator. Then we directly fitted $g_2(\tau)$ using a constrained regularization method, which is included in the ALV software. The mathematical background of regularization DLS data is precisely described in the CONTIN 2DP program by Provencher[1,2]. Equation S.2 shows the ALV nonlinear fit model for calculating smooth distribution functions

$$g_2(\tau) - 1 = \left(\int_{\Gamma_{min}}^{\Gamma_{max}} e^{-\Gamma\tau} G(\Gamma) d\Gamma \right)^2 , \tag{S.2}$$

where $G(\Gamma)$ denotes the distribution function of the decay rate Γ. The decay rate itself coheres with the diffusion coefficient D through $\Gamma = Dq^2$, while $q = \frac{4\pi n}{\lambda} \sin\frac{\theta}{2}$ describes the scattering vector including the solvent refractive index (n) and the laser wavelength (λ). Under the assumption that i) scattering particles behave as hard spheres in dilute solution and ii) Rayleigh-Debye theory is valid, the Stokes-Einstein-equation (equation S.3) allows calculating the distribution of the hydrodynamic radius R_H based on

$$D = \frac{k_B T}{6\pi\eta R_H}, \tag{S.3}$$

considering the Boltzmann constant k_B, the temperature T and the solvent viscosity η. The final 'mass weighted' particle radius distribution function results in adjusting the amplitudes of the decay rate in order to cut unphysically large contributions at small particle radii.

The Litesizer 500 with three different scattering angles ($15°, 90°, 175°$) uses a correlator, which can perfom up to 248 auto/cross-correlations simultaneously over a time-range of $10\,\text{ns}$ to $85\,\text{s}$. As a result, we again obtained the intensity time correlation function $g_2(\tau)$, but here we have to deal with a slightly different algorithm. The Kalliope Software contains a 'non-negative least square' (NNLS) fitting routine with Tikhonov regularization[3,4]. In addition, we could decide between the options 'general' and 'narrow', which influence the regularization parameter of the Thikonov-NNLS. We chose the latter variation, because of the smaller peak width in the calculated particle radius distribution function. Furthermore, we used the 'volume weighted' particle size distribution function in order to report analogous results compared to the ALV measurements.

Independently from the DLS device we measured all samples with a quality setup of 6 runs, where each run took $30\,\text{s}$ and all runs were averaged into one intensity time correlation function. Next to correlation functions and particle radius distributions we also looked at the behavior of the mean scattering intensity or mean count rate. The adjustments for the laser attenuation, which have a direct impact on the mean scattering intensity, were carried out automatically in order to detect optimized

count rate traces. Therefore we will always specify the current laser attenuation while presenting these values.

Continuous Wave Electron Paramagnetic Resonance (CW EPR) Spectroscopy measurements

X-band CW EPR measurements, which were performed with the Miniscope MS400, made use of a sweep width of 100 G, a modulation amplitude of 600 mG and a microwave attenuation of 20 dB. Note that the modulation amplitude surpassed the standard limit of $< 0.5\ B_{pp}$ (B_{pp} as peak-to-peak line width) to gain spectra with a improved phase resolution. Q-band CW EPR measurements were carried out with the Bruker EMX-plus spectrometer. We applied the same microwave attenuation as written before, but used a sweep width of 130 G and a modulation amplitude of 1000 mG.

The important step for our simulation approach, which is based on the slow-motion theory developed by Schneider and Freed[5], was to choose suitable starting parameters for Fremy's salt g-tensor and hyperfine coupling tensor A. The spectral simulations were performed in Matlab (R2016a, v. 9.0) exploiting the EasySpin package (v. 5.1.10)[6]. Based on literature data[7] we took the following parameter sets:

- g-tensor: $g_{xx} = 2.0086$, $g_{yy} = 2.0064$, $g_{zz} = 2.0029$

- hyperfine-tensor (X-band): $A_{xx} = 5.3\,\text{G}$, $A_{yy} = 5.5\,\text{G}$, $A_{zz} = 28.3\,\text{G}$

- hyperfine-tensor (Q-band): $A_{xx} = 5.5\,\text{G}$, $A_{yy} = 5.6\,\text{G}$, $A_{zz} = 28.3\,\text{G}$

Other values like line broadening and rotational diffusion rates that have to be implied into the simulation routine, depend significantly on the solvent composition and will be characterized while analysing the CW EPR spectra. For calculating the rotational correlation time τ_c (see equation S.4), we sticked to a simple model of Brownian diffusion with an axial rotational diffusion tensor containing the values $D_\parallel$ (unique axis) and $D_\perp$ (perpendicular to the unique axis)[8]

$$\tau_c = \frac{1}{6\sqrt[3]{D_\perp^2 D_\parallel}} \quad . \tag{S.4}$$

The discussed informations about the line width of all measured CW EPR spectra (see main text) are based on isotropic broadening, which is implemented in the EasySpin program package. Note that this method does not assume any physical model causing the broadening. Instead we compared the full width at half maximum (FWHM) values of pure Fremy's salt with $\mathbf{1}^{4+}$:$\mathbf{3}^{2-}$ in every investigated solvent or bulk concentration to further specify the effect of the cation $\mathbf{1}^{4+}$.

Besides calculating the rotational correlation time τ_c as well as determine the isotropic broadening, we established a routine to analyse the present anisotropy of the rotational diffusion tensor. Note that even paramagnetic molecules in the 'fast-motion regime' significantly reflect deviations from the

isotropic case through their CW EPR spectra.[8]. Based on the rotational diffusion tensor containing $D_\parallel$ and $D_\perp$, we calculated its anisotropy T using equation S.5

$$T = \frac{D_\parallel - D_\perp}{D_\parallel + 2D_\perp} \quad . \tag{S.5}$$

A larger T-value indicates stronger separation between $D_\parallel$ and $D_\perp$, while smaller T-values reflect more isotropic tumbling, which can be attributed to weaker electrostatic interactions in the direct vicinity. For ion clouds with later self-assembly into globular *ionoids* the right balance between attractive and repulsive electrostatic forces is important, which translates into an anisotropy T that must be situated in a specific range. Based on the established system[9] we know the anisotropy preceding formation of *ionoids* and use it as a reference for all tested solvent mixtures and bulk concentrations. Finally, we had to imply so-called Euler angles α, β and γ to simulate CW EPR spectra at both frequencies with the EasySpin package. The main text already points out the principal axis of fast rotation for pure Fremy's salt and the system $\mathbf{1}^{4+}{:}\mathbf{3}^{2-}$; the entire set of Euler angles is made out of:

- pure Fremy's salt: $\alpha = 65°$, $\beta = 90°$, $\gamma = 15°$ and

- $\mathbf{1}^{4+}{:}\mathbf{3}^{2-}$: $\alpha = 85°$, $\beta = 90°$, $\gamma = 15°$.

Modifying solvent volume stoichiometry

a) DLS results

Fig. S.1 contains the remaining volume stoichiometries, which were left out in the main text. The solvent mixtures with increasing amount of DMSO do not show a correlation between the solvent composition and the development of the hydrodynamic radius at any given measurement day. Furthermore, we recognize a rather large fluctuation in the R_H-values in all solvent mixtures for the system $\mathbf{1}^{4+}{:}\mathbf{2}^{2-}$, indicating the absence of highly-defined structures. It seems that the $\mathbf{1}^{4+}$- and $\mathbf{2}^{2-}$-ion are more or less settled in the initial ion cloud state.
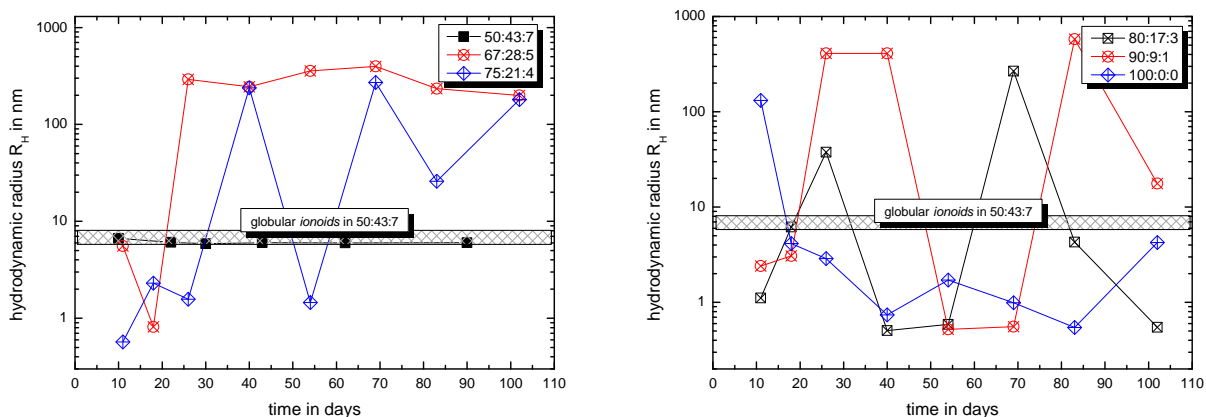
Fig. S.1: Development of the hydrodynamic radius for the cluster system $\mathbf{1}^{4+}$:$\mathbf{2}^{2-}$ at a ratio of 1 mM : 3 mM. We divided the results of the volume stoichiometries with increasing DMSO amount into two graphs for clarity: on the left stoichiometries 67:28:5 and 75:21:4 and on the right 80:17:3 to 100:0:0. Both graphs contain a patterned box that highlights the region of the hydrodynamic radius for the established solvent mixture. Additionally, the left graph contains the DLS data for the 50:43:7 solvent mixture as reference.

Fig. S.2 contains the intensity time correlation and particle radius distribution function for $\mathbf{1}^{4+}$:$\mathbf{2}^{2-}$ dissolved in the volume stoichiometries with decreasing amount of DMSO (33 vol.-% to 10 vol.-%) at measurement day 11. We detect that all four intensity time correlation functions decay at almost the same correlation time, indicating the existence of at least one particle type with similar size. This trend corresponds with the particle radius distributions, implying a strong dependency of the decay rate by the second entity with $R_H \approx 150$ nm. Furthermore, the y-intercept of the intensity time correlation function decreases with the amount of DMSO in the solvent mixture. This behavior coheres with the changing mass fraction for both sample entities. The volume stoichiometries 33 vol.-% to 10 vol.-% show that the weighting in the particle radius distribution shifts from the second to the first peak. These self-assembled structures with their small size deliver, based on the Rayleigh theory, a reduced mean scattering intensity, which significantly effects the intensity time correlation function.
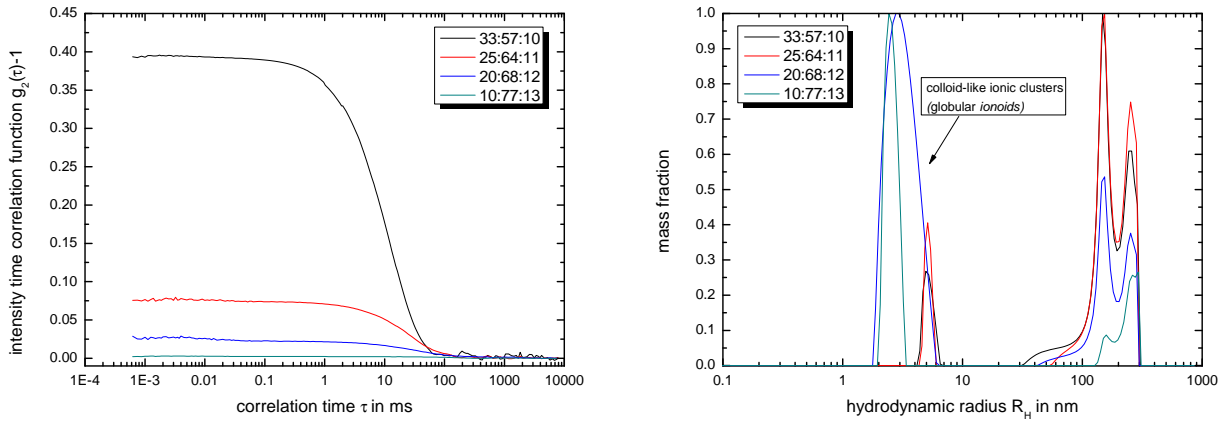
Fig. S.2: Intensity time correlation function (left) and particle radius distribution function (right) for 1^{4+}:2^{2-} in the solvent mixtures DMSO:glycerol:water with decreasing amount of DMSO (33 vol.-% to 10 vol.-%) at measurement day 11.

Besides characterizing the four volume stoichiometries with decreasing amount of DMSO, we want to highlight the long-term stability for one solvent mixture. Fig. S.3 displays the development of the intensity time correlation function and the mean scattering intensity through the total measurement time for 1^{4+}:2^{2-} in DMSO:glycerol:water 33:57:10 (v/v/v).
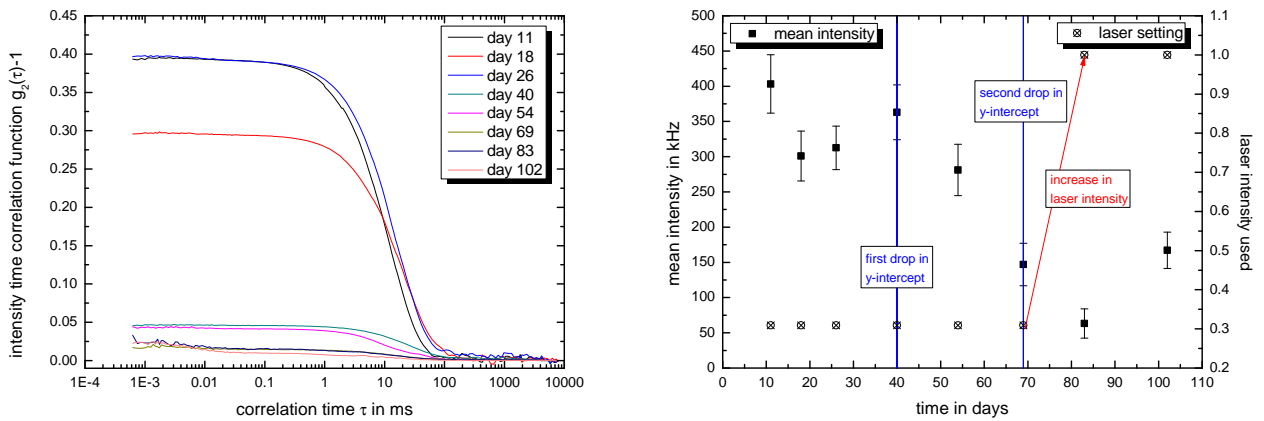
Fig. S.3: Intensity time correlation function (left) and mean scattering intensity with laser settings (right) for 1^{4+}:2^{2-} in DMSO:glycerol:water 33:57:10 in dependence of the measurement time.

The intensity time correlation functions show two major drops in their y-interceps at day 40 and day 69, which are also marked in the diagram with the mean scattering intensity. For day 40 we do not see significant changes in the mean count rate, but the particle radius distribution indicates the beginning decomposition of the present anisotropic ionic clusters. The second drop however coheres

8

with the decreasing mean scattering intensity, which implies the abscence of highly defined structures inside the solution. To support the permanent character of this radical change, we expanded the DLS measurements till day 102. Furthermore, we had to increase the laser intensity (maximum value of 1.0) for the last two measurements in order to maintain the mean count rate. In general, we can evaluate the stability of colloid-like ionic clusters through comparing the intensity time correlation function with the associated mean scattering intensity.

b) CW EPR results
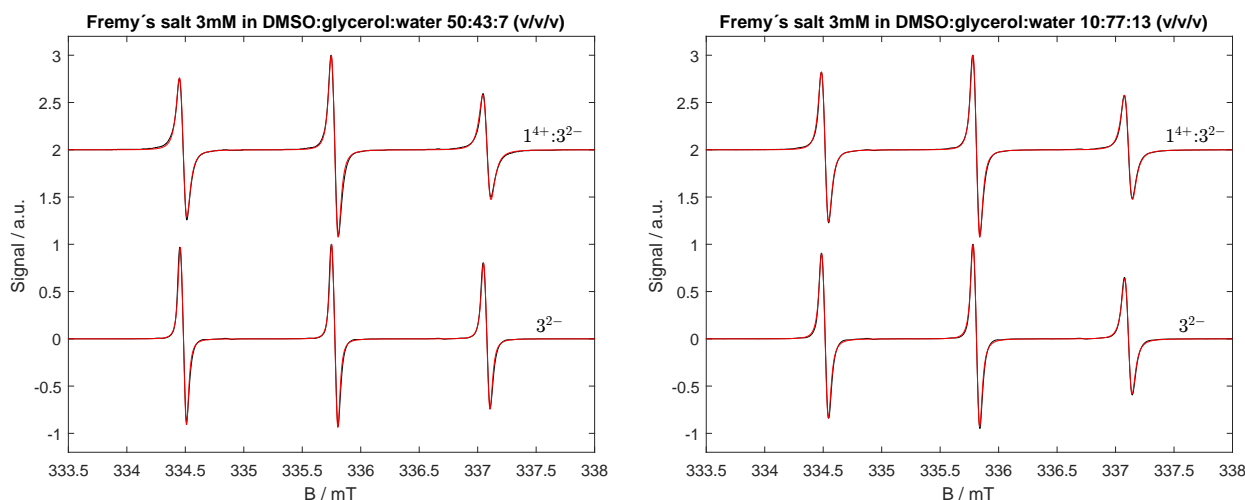
Fig. S.4: Left: X-band CW EPR spectra of Fremy's salt 3 mM and $\mathbf{1}^{4+}$:$\mathbf{3}^{2-}$ in DMSO:glycerol:water 50:43:7 (v/v/v). Right: X-band CW EPR spectra for the same components in DMSO:glycerol:water 10:77:13 (v/v/v). Both graphs contain the experimental data as black lines and the simulated data as red lines.

Based on the rotational mobility of Fremy's salt in the established solvent mixture DMSO:glycerol:water 50:43:7 (v/v/v), we received a reference diffusion tensor at X-Band frequencies (see Table S.4). The increase of glycerol in the solvent mixture causes due to the higher viscosity a hindered rotational mobility of pure Fremys's salt, which leads to smaller $D_\perp$ and $D_\parallel$ values. In addition to that, the $\mathbf{1}^{4+}$:$\mathbf{3}^{2-}$ system does effect the rotational mobility around the molecular z-axis. This variation is also visible in the behavior of the anisotropy T, where both X- and Q-band data show the same tendencies (see Fig. S.5).
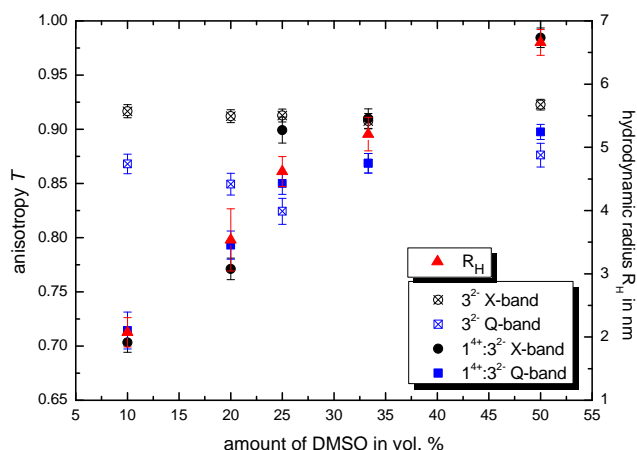
Fig. S.5: Plot of the anisotropy T (equation S.5) of pure Fremy's salt and system 1^{4+}:3^{2-} for X-and Q-band against the amount of DMSO in the solvent. The red triangles show the behavior of the hydrodynamic radius of 1^{4+}:2^{2-} at day 11.

The anisotropy of the pure Fremy's salt displays only minor changes with reducing amount of DMSO inside the solvent mixture. Note that the reduced anisotropy at Q-band frequencies correlates with the difference in frequency/field dependence of the rotational time-frame with higher frequencies/magnetic fields, just like the spectra in the main text visualize exemplary. Furthermore, we see an outstanding decay in the anisotropy for the system 1^{4+}:3^{2-} throughout all tested volume stoichiometries. We can exclude solvent viscosity as cause for this behavior, as we then would also have to observe this trend with pure Fremy's salt, leaving electrostatic interactions as origin. Reducing the amount of DMSO in the solvent mixture decreases the electrostatic interactions between 1^{4+} and 3^{2-}, which creates a more isotropic environment for Fremy's salt and a less pronounced difference between $D_{\perp}$ and $D_{\parallel}$. Besides the decrease in DMSO content, we increase the water content inside the solvent mixture, inducing partially solvated Fremy's salt molecules in this region as well as lower T-values. In general, we can correlate the trend of the anisotropy in the ion clouds and the hydrodynamic radius of the self-assembled structures.

Table S.4 combines all simulated $D_{\perp}$ and $D_{\parallel}$ values for pure Fremy's salt as well as the system 1^{4+}:3^{2-} that were used to calculate the rotational correlation time τ_c (equation S.4) as well as the rotational anisotropy T. The results for pure Fremy's salt with the tested solvent mixtures are expanded with data of 3^{2-} in pure water, DMSO and glycerol 88 wt%.

Table S.4: Summary of the simulated axial rotational diffusion tensor $D_\perp$ and $D_\parallel$ as well as the calculated rotational correlation time τ_c and anisotropy T for pure Fremy's salt and 1^{4+}:3^{2-} at X-band frequencies while changing the volume stoichiometry of the solvent mixture DMSO:glycerol:water

solvent	3^{2-}				1^{4+}:3^{2-}			
	$D_\perp$ / s^{-1}	$D_\parallel$ / s^{-1}	τ_c / ps	T	$D_\perp$ / s^{-1}	$D_\parallel$ / s^{-1}	τ_c / ps	T
50:43:7	9.5e8	3.5e10	52.72	0.923	2.1e8	4.0e10	137.94	0.984
33:57:10	4.6e8	1.4e10	116.05	0.908	3.2e8	1.0e10	165.35	0.910
25:64:11	3.4e8	1.1e10	153.84	0.913	2.7e8	7.5e9	203.82	0.899
20:68:12	2.8e8	9.0e9	187.21	0.912	3.6e8	4.0e9	207.47	0.771
10:77:13	2.5e8	8.5e9	205.79	0.917	3.7e8	3.0e9	224.22	0.703
0:0:100	3.0e10	6.0e10	4.41	0.250	-	-	-	-
100:0:0	4.0e9	4.0e10	19.34	0.750	-	-	-	-
0:85:15	2.0e8	7.0e9	254.76	0.919	-	-	-	-

At Q-band frequencies, the behavior of the rotational anisotropy T of 1^{4+}:3^{2-} and pure Fremy's salt is analogous to the X-band data and therefore will not be explained separatly. However, Fig. S.6 contains the measured Q-band CW EPR spectra with decreasing amount of DMSO inside the solvent mixture (50 vol.-% to 10 vol.-%).

Pure Fremy's salt delivers the expected trend with increasing amount of glycerol in the solvent mixture; the rotational mobility of the nitroxide declines due to the rising solvent viscosity. Adding 1^{4+} results in further restriction for the rotational mobility of 3^{2-} and broader linewidths due to electrostatic interactions. Table S.5 combines, equivalent to the X-band results, the important values from our simulations/calculations. However, the rotational correlation times τ_c from 1^{4+}:3^{2-} in DMSO:glycerol:water 25:64:11 and 20:68:12 (v/v/v) surpass significantly the values for all the other listed solvents. In contrary, the anisotropy does not rise, because of the simultaneous drop of $D_\perp$ and $D_\parallel$. One reason for this special behavior can be found in stronger local electrostatic interactions between 1^{4+} and 3^{2-} due to local aberrations in the solvent compositions from the macroscopic ratio inside the ion cloud.
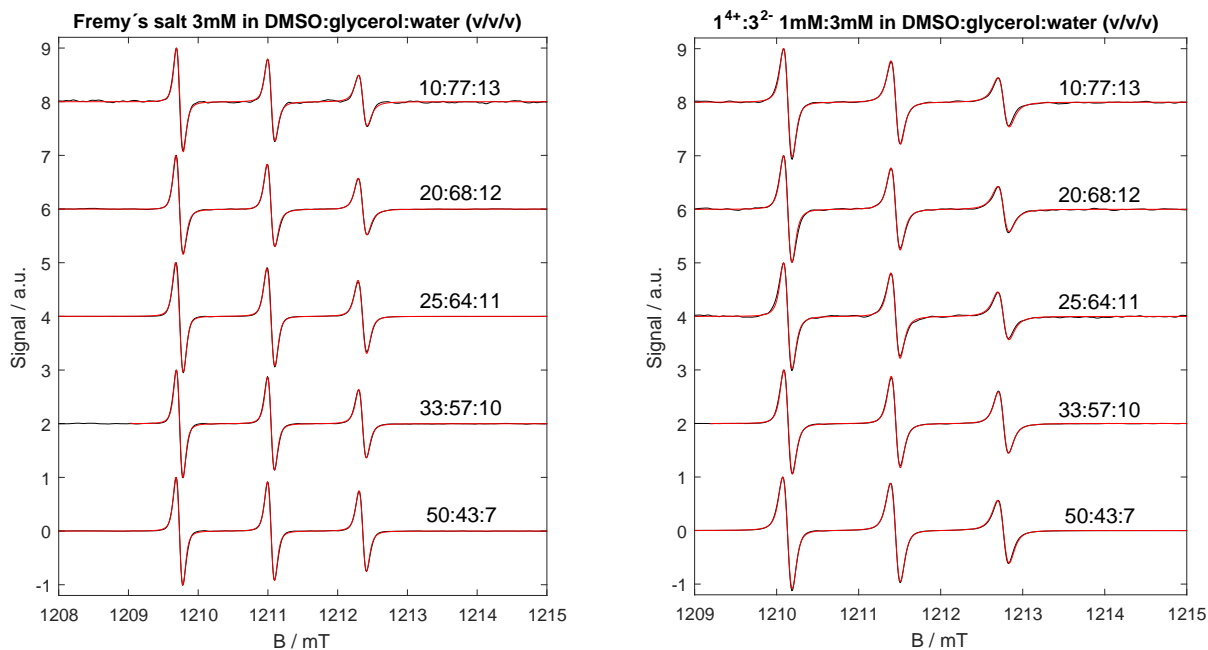
Fig. S.6: Q-band CW EPR specra of Fremy's salt (left) and $\mathbf{1}^{4+}$:$\mathbf{3}^{2-}$ (right) in DMSO:glycerol:water with decreasing amount of DMSO (50 vol.-% to 10 vol.-%). Again we illustrate the experimental data with black lines and the simulated data with red lines.

Table S.5: Summary of the simulated axial rotational diffusion tensor $D_\perp$ and $D_\parallel$ as well as the calculated rotational correlation time τ_c and anisotropy T for pure Fremy's salt and $\mathbf{1}^{4+}$:$\mathbf{3}^{2-}$ at Q-band frequencies while changing the volume stoichiometry of the solvent mixture DMSO:glycerol:water

solvent	$\mathbf{3}^{2-}$				$\mathbf{1}^{4+}$:$\mathbf{3}^{2-}$			
	$D_\perp$ / s^{-1}	$D_\parallel$ / s^{-1}	τ_c / ps	T	$D_\perp$ / s^{-1}	$D_\parallel$ / s^{-1}	τ_c / ps	T
50:43:7	9.0e8	2.0e10	65.87	0.876	3.3e8	9.0e9	167.79	0.898
33:57:10	7.2e8	1.5e10	84.13	0.869	3.6e8	7.5e9	168.25	0.869
25:64:11	6.5e8	9.8e9	103.79	0.824	2.5e8	4.5e9	254.38	0.850
20:68:12	5.3e8	9.5e9	120.16	0.849	2.8e8	3.5e9	256.48	0.793
10:77:13	4.1e8	8.5e9	147.97	0.868	4.0e8	3.4e9	204.17	0.714
0:0:100	3.6e10	6.2e10	3.86	0.194	-	-	-	-
100:0:0	7.0e9	3.5e10	13.92	0.571	-	-	-	-
0:85:15	3.5e8	5.0e9	196.25	0.816	-	-	-	-

Modifying glycerol:water volume ratio

a) DLS results

Based on the description in the main text, Fig. S.7 displays the intensity time correlation functions at day 7 and day 14 for selected solvent compositions. Here we chose at least one mixture out of each DMSO:glycerol:water (v/v/v) region:

1. 50:5:45 to 50:15:35

2. between 50:15:35 and 50:40:10

3. between 50:40:10 and 50:45:5

4. above 50:45:5.

a)
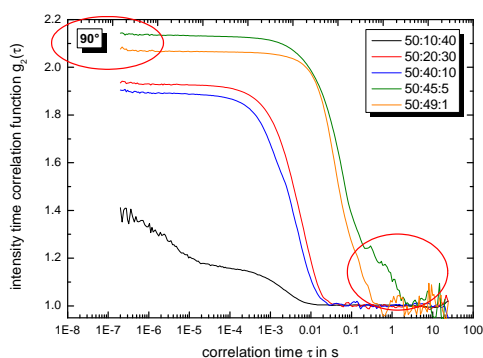
c)
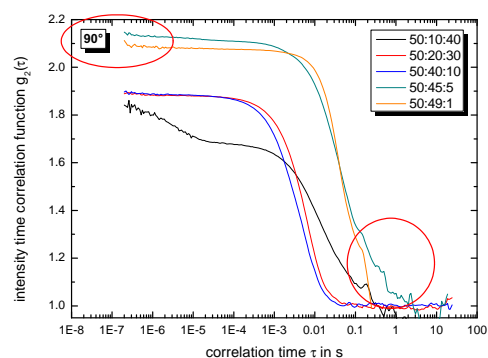
b)
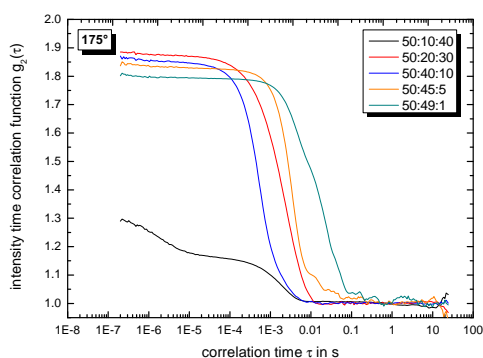
d)
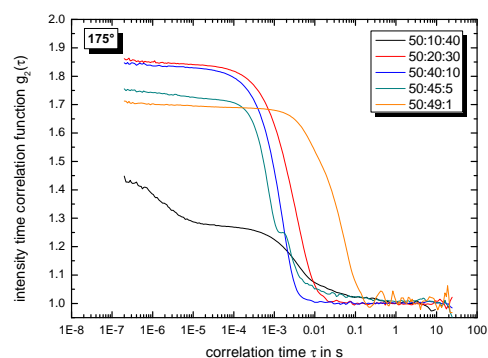
Fig. S.7: a)-d) Intensity time correlation function of $\mathbf{1}^{4+}$:$\mathbf{2}^{2-}$ 1 mM:3 mM in solvent mixtures with various DMSO:glycerol:water (v/v/v) ratios. a)-b) Results from day 7 with side- and backscattering. c)-d) Results from day 14 with side- and backscattering.

Note that the defined regions are based on the first three weeks for the system $\mathbf{1}^{4+}$:$\mathbf{2}^{2-}$ 1 mM:3 mM in each solvent mixture. The self-assembly into globular *ionoids* in DMSO:glycerol:water 50:43:7

(v/v/v) takes 10 days, permitting the preliminary performed classification. However, it is difficult to derive their long-term stability, which is not the main emphasis of these DLS measurements. We focus on the beginning of the self-assembly process, which is crucial for the formation of well-defined structures.

The solvent mixture DMSO:glycerol:water 50:10:40 (v/v/v) does not form highly-defined self-assembled structures, which is already visible in the weakly pronounced intensity time correlation functions. Furthermore, the trend of these graphs stays constant throughout the measuring time even at different scattering angles, implying a stagnation at the ion cloud state. Increasing the amount of glycerol in the solvent mixture helps building anisotropic ionic clusters throughout the entire solution, which results in nicely shaped intensity time correlation functions. However, at the ratio of 50:40:10 (v/v/v) we detect (for both scattering angles) a shift of these graphs to lower correlation times. This indicates the formation of smaller aggregates and leads to highly defined globular *ionoids* in the solvent mixture DMSO:glycerol:water 50:43:7 (v/v/v).

Further changes in the glycerol:water ratio towards higher amounts of glycerol invert the movement for the intensity time correlation function. At sidescattering we also detect intensity time correlation functions with an elevated baseline as well as larger y-intercept values than 2 (see the red circles in Fig. S.7). These features hint out the existence of number fluctuations. Number fluctuations occur, when a small amount of larger particles pass the laser, while the remaining solution provides only minor scattering intensity. The system 1^{4+}:2^{2-} initiates from large ion cloud formations, but also keeps a minor potential to form at least anisotropic ionic clusters. Due to these variations in the hydrodynamic radius, the detection of number fluctuations seems likely possible.

b) CW EPR results

Similar to the first solvent mixtures we measure a correlation between the hindered rotational mobility for pure Fremy's salt with increasing viscosity or amount of glycerol. Through adding 1^{4+} we determine an additional slow-down for 3^{2-} (see Fig. S.8 and S.10), which results in a reduced $D_\perp$ tensor.
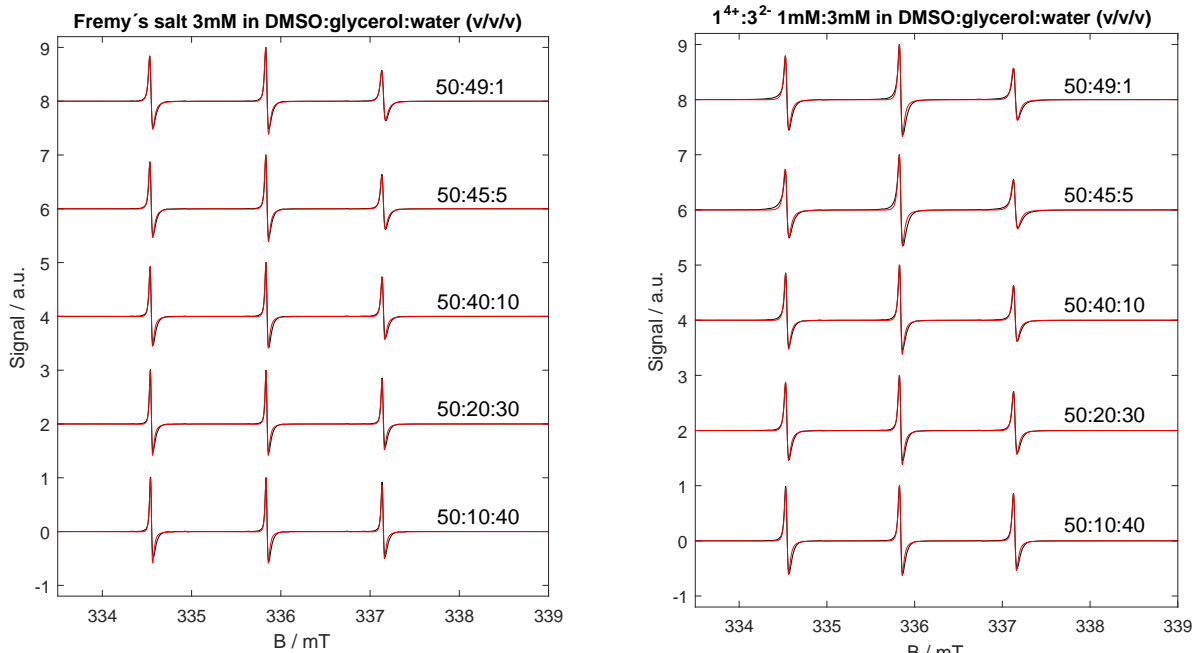
Fig. S.8: X-band CW EPR specra of Fremy's salt (left) and 1^{4+}:3^{2-} (right) in various DMSO:glycerol:water (v/v/v) ratios containing both experimental (black lines) as well as simulated data (red lines).

The development of the rotational dynamics anisotropy-values of pure Fremy's salt and especially 1^{4+}:3^{2-} for X- and Q-band do not provide four different regions as we observed them with DLS, as Fig. S.9 demonstrates. This is different compared to the line width analysis in the main text, which provides similar regions compared to our light scattering method.

Pure Fremy's salt at X-band frequencies clearly displays a steady increase in T beginning at the glycerol:water-ratio 15:35, when increasing the glycerol and decreasing the water content in the solvent mixture. As a result, we just see the expected slow-down in axially symmetric rotational motion when increasing the solvent viscosity. Again the difference in frequency/field dependence of the rotational time-frame becomes apparent when looking at the Q-band data. Here the increase in the T-value only starts at glycerol:water 40:10.

With adding the 1^{4+}, we detect a significant increase in the anisotropy thoughout all solvent mixtures and at both CW EPR frequencies. Furthermore, the T-values do not contain the correlation with solvent viscosity as seen for pure Fremy's salt. The effects of the i) electrostatic interactions between 1^{4+} and 3^{2-} and the ii) constant amount of DMSO inside the solvent mixture are strong enough, to overlay the influence of the glycerol:water-ratio. Thus the volume ratio of glycerol and water determines mainly the size and shape of the self-assembled structures, but not a specific behavior for the anisotropy T.

15
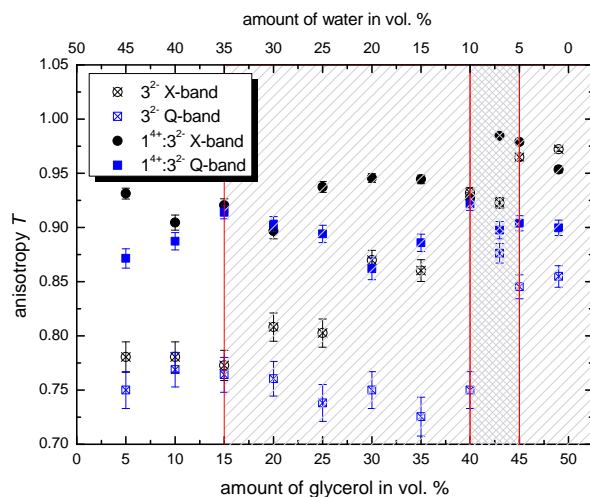
Fig. S.9: Plot of the anisotropy T (equation S.5) of pure Fremy's salt and system $\mathbf{1}^{4+}$:$\mathbf{3}^{2-}$ for X- and Q-band against the amount of glycerol and water in volume percentage. The regions marked in different shadings are based on the DLS data as described in the main text.

Table S.6 summarizes, equal to the first section, the important parameters for calculating τ_c and T. A closer look at the rotational correlation times for $\mathbf{1}^{4+}$:$\mathbf{3}^{2-}$ reveals a significant increase of τ_c at solvent mixture DMSO:glycerol:water 50:15:35 (v/v/v). Based on the DLS data we know that this solvent marks the starting point for creating at least anisotropic ionic clusters. Thereby we can associate the increase of τ_c with stronger globular electrostatic interactions between $\mathbf{1}^{4+}$ and $\mathbf{3}^{2-}$ inside the ion cloud state, which are important to form highly defined self-assembled structures. The other regions that were characterized with DLS, can not be distinguished through CW EPR at X-band frequencies due to the restriction of analysing the initial ion cloud.

Utilizing Q-band frequencies, the behavior of the rotational anisotropy T of $\mathbf{1}^{4+}$:$\mathbf{3}^{2-}$ and pure Fremy's salt is in most parts analogous with the X-band results and was already discussed. The Q-band CW EPR spectra (Fig. S.10) deliver for solely $\mathbf{3}^{2-}$ the familiar correlation between rotational mobility and solvent viscosity. The same can be determined while adding the $\mathbf{1}^{4+}$ with the exception for solvent mixtures DMSO:glycerol:water 50:45:5 and 50:49:1 (v/v/v). The first mixture displays an additional slow-down for the rotational mobility of Fremy's salt, which is already visible in the highfield peak of the CW EPR spectra (see Fig. S.10). A further increase of glycerol inside the solvent cancels the effect and provides rotational correlation times in the region of DMSO:glycerol:water 50:40:10 (v/v/v). Note that this additional phenomena occurs with solvent mixture, where we found based on the DLS results the potential to form globular *ionoids*. The initial ion cloud seems to induce stronger local electrostatic interactions between $\mathbf{1}^{4+}$ and $\mathbf{3}^{2-}$, which are on the one hand only detectable at higher frequencies/magnetic fields and on the other hand important to create either future anisotropic ionic clusters or globular *ionoids*. The exact values for $D_\perp$, $D_\parallel$, τ_c and T are written down in Table S.7.

Table S.6: Summary of the simulated axial rotational diffusion tensor $D_\perp$ and $D_\parallel$ as well as the calculated rotational correlation time τ_c and anisotropy T for pure Fremy's salt and $\mathbf{1^{4+}}{:}\mathbf{3^{2-}}$ at X-band frequencies while changing the glycerol:water ratio of the solvent mixtures

solvent	$\mathbf{3^{2-}}$				$\mathbf{1^{4+}}{:}\mathbf{3^{2-}}$			
	$D_\perp$ / s^{-1}	$D_\parallel$ / s^{-1}	τ_c / ps	T	$D_\perp$ / s^{-1}	$D_\parallel$ / s^{-1}	τ_c / ps	T
50:5:45	3.0e9	3.5e10	24.50	0.780	1.2e9	5.0e10	40.06	0.931
50:10:40	3.0e9	3.5e10	24.50	0.780	1.7e9	5.0e10	31.76	0.904
50:15:35	2.5e9	2.8e10	29.80	0.773	7.0e8	2.5e10	72.30	0.920
50:20:30	2.2e9	3.0e10	31.71	0.808	7.4e8	2.0e10	75.05	0.897
50:25:25	2.5e9	3.3e10	28.21	0.803	6.1e8	2.8e10	76.31	0.937
50:30:20	1.9e9	4.0e10	31.68	0.870	4.7e8	2.5e10	94.29	0.946
50:35:15	1.9e9	3.7e10	32.60	0.860	5.0e8	2.6e10	89.31	0.944
50:40:10	9.5e8	4.0e10	50.43	0.932	4.6e8	1.8e10	106.72	0.927
50:45:5	4.8e8	4.0e10	79.49	0.965	2.5e8	3.5e10	128.39	0.979
50:49:1	3.8e8	4.0e10	92.89	0.972	3.2e8	2.0e10	131.24	0.953

Table S.7: Summary of the simulated axial rotational diffusion tensor $D_\perp$ and $D_\parallel$ as well as the calculated rotational correlation time τ_c and anisotropy T for pure Fremy's salt and $\mathbf{1^{4+}}{:}\mathbf{3^{2-}}$ at Q-band frequencies while changing the glycerol:water ratio of the solvent mixtures

solvent	$\mathbf{3^{2-}}$				$\mathbf{1^{4+}}{:}\mathbf{3^{2-}}$			
	$D_\perp$ / s^{-1}	$D_\parallel$ / s^{-1}	τ_c / ps	T	$D_\perp$ / s^{-1}	$D_\parallel$ / s^{-1}	τ_c / ps	T
50:5:45	4.5e9	4.5e10	17.19	0.750	1.5e9	3.2e10	40.06	0.871
50:10:40	4.1e9	4.5e10	18.30	0.780	1.3e9	3.2e10	44.07	0.887
50:15:35	4.2e9	4.5e10	18.00	0.764	7.6e8	2.5e10	68.44	0.914
50:20:30	3.8e9	4.0e10	20.01	0.761	7.6e8	2.2e10	71.42	0.903
50:25:25	3.7e9	3.5e10	21.30	0.738	7.6e8	2.0e10	73.73	0.894
50:30:20	3.3e9	3.3e10	23.44	0.750	7.1e8	1.4e10	86.89	0.862
50:35:15	2.8e9	2.5e10	28.69	0.725	7.0e8	1.7e10	82.22	0.886
50:40:10	2.0e9	2.0e10	38.68	0.750	3.3e8	1.2e10	152.45	0.922
50:45:5	9.2e8	1.6e10	69.93	0.845	2.5e8	7.3e9	216.50	0.904
50:49:1	7.5e8	1.4e10	83.77	0.854	4.3e8	1.2e10	127.78	0.900
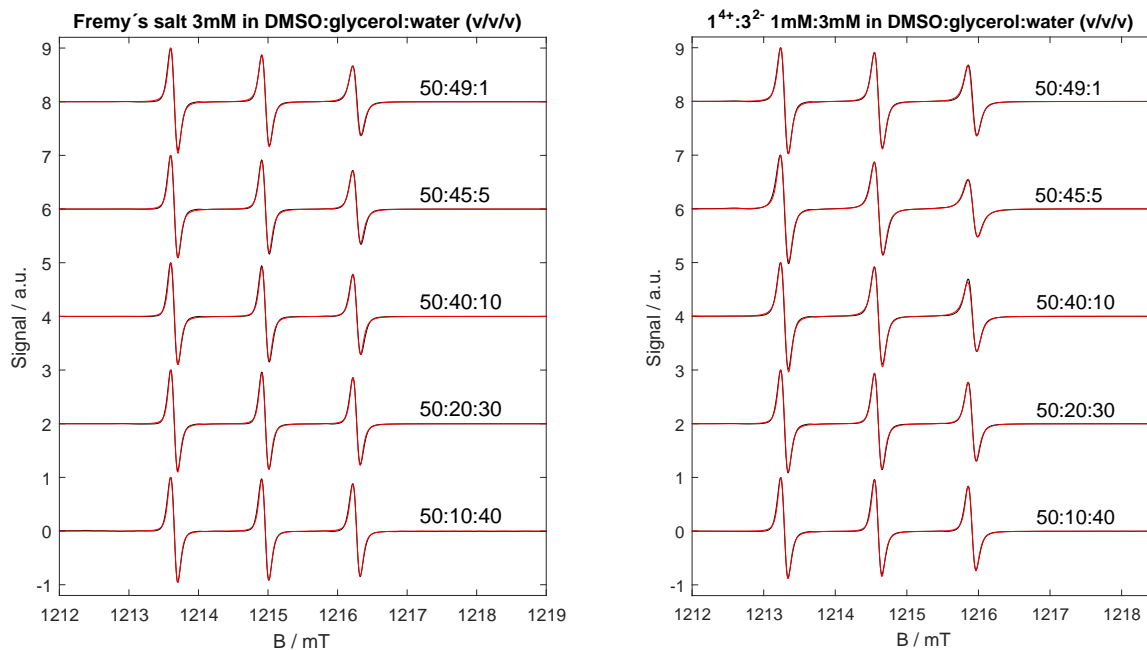
Fig. S.10: Q-band CW EPR specra of Fremy's salt (left) and $\mathbf{1^{4+}}$:$\mathbf{3^{2-}}$ (right) in various DMSO:glycerol:water (v/v/v) ratios containing both experimental (black lines) as well as simulated data (red lines).

Importance of bulk concentration

a) DLS results

Based on the declarations in the main text, we divide Fig. S.11 into bulk concentrations, which are able to build at least anisotropic ionic clusters with the system $\mathbf{1^{4+}}$:$\mathbf{2^{2-}}$ in DMSO:glycerol:water 50:43:7 (v/v/v) and compositions that remain mainly in the ion cloud state. The important transition point is the 'critical *ionoid* concentration' between 0.1 mM:0.3 mM and 0.2 mM:0.6 mM. Higher bulk concentrations contain enough $\mathbf{1^{4+}}$- and $\mathbf{2^{2-}}$-ions to induce the formation of highly defined self-assembled structures.

$\mathbf{1^{4+}}$:$\mathbf{2^{2-}}$ with bulk concentration 1 mM:3 mM and lower were observed for 45 days i) to highlight the crucial initial state for the formation of globular *ionoids* and ii) to check the stability of the structures through the mean scattering intensity. The second fact delivered stable values after the formation of the two separated entities at lower bulk concentrations was fulfilled. Furthermore, we can describe the change of globular *ionoids* to anisotropic ionic clusters using the mean scattering intensity (see Fig. S.11). Based on the results on day 10 we recognize two facts:

1. a drop in the mean scattering intensity and

2. an increase in the used laser power at bulk concentration 0.2 mM:0.6 mM.

Both aspects imply a significant loss in the overall arrangement of $\mathbf{1^{4+}}$ and $\mathbf{2^{2-}}$, which is equated with the transformation from monodisperse globular *ionoids* to anisotropic ionic clusters.
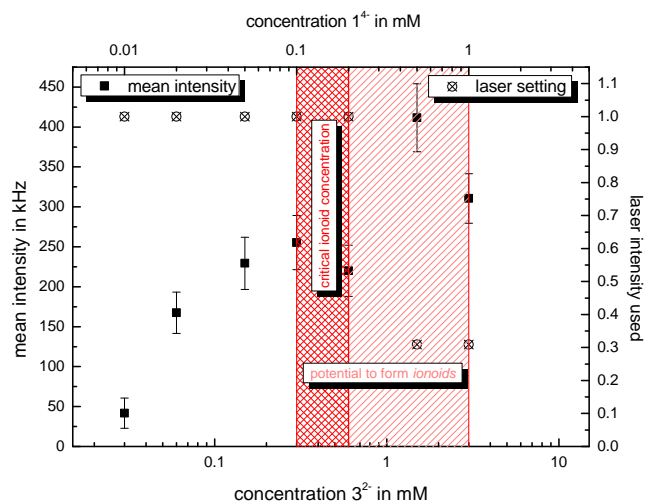
Fig. S.11: Mean scattering intensity with laser settings at day 10 for the system $\mathbf{1}^{4+}$:$\mathbf{2}^{2-}$ in DMSO:glycerol:water 50:43:7 (v/v/v) dependent on the bulk concentration. The light red patterned box highlights the concentration region with the potential to form anisotrop ionic clusters as well as globular *ionoids*, while the red patterned box displays the 'critical *ionoid* concentration'.

Bulk concentrations below the 'critical *ionoid* concentration' can not self-assemble into well-defined structures throughout the entire solution due to weaker electrostatic interactions between $\mathbf{1}^{4+}$ and $\mathbf{2}^{2-}$. Therefore, we detect mainly ion clouds, which deliver lower mean scattering intensities. Note that here the mean scattering intensity decreases almost linear with reducing bulk concentration, which indicates a steady modification from a defined $\mathbf{1}^{4+}$:$\mathbf{2}^{2-}$-structure to homogeneously distributed ions. In general, using mean scattering values allows us to track the smooth transition from globular *ionoids* over anisotropic ionic clusters to ion clouds.

The second experiment, which includes the highest tested bulk concentration of 1.5 mM:4.5 mM was left out in Fig. S.11, because it was not recorded with the same DLS device. In addition, we measured this sample just for 28 days due to its reliable mean scattering intensity and absent formation of two separated entities.

b) CW EPR results

Table S.8 summarizes the simulated values of $D_\perp$ and $D_\parallel$ as well as the calculated rotational correlation times τ_c and rotational anisotropy T for all tested bulk concentrations at X-band frequencies. Analogous to the X-band results, Table S.9 combines the data of $D_\perp$, $D_\parallel$, τ_c and T at Q-band frequency for all tested bulk concentrations.

Table S.8: Summary of the simulated axial rotational diffusion tensor $D_\perp$ and $D_\parallel$ as well as the calculated rotational correlation time τ_c and anisotropy T for pure Fremy's salt and $\mathbf{1}^{4+}{:}\mathbf{3}^{2-}$ in DMSO:glycerol:water 50:43:7 (v/v/v) at X-band frequencies while changing the bulk concentration

| c-ratio | $\mathbf{3}^{2-}$ | | | | $\mathbf{1}^{4+}{:}\mathbf{3}^{2-}$ | | | |
mM:mM	$D_\perp$ / s^{-1}	$D_\parallel$ / s^{-1}	τ_c / ps	T	$D_\perp$ / s^{-1}	$D_\parallel$ / s^{-1}	τ_c / ps	T
1.5:4:5	9.0e8	3.5e10	54.66	0.927	2.3e8	4.0e10	129.82	0.983
0.5:1:5	9.5e8	3.5e10	52.72	0.923	1.8e8	5.0e10	141.91	0.989
0.2:0.6	8.0e8	3.7e10	58.04	0.938	2.1e8	4.0e10	137.94	0.984
0.1:0.3	7.2e8	4.0e10	60.65	0.948	2.2e8	4.0e10	133.73	0.975
0.05:0.15	8.5e9	3.5e10	56.78	0.934	3.4e8	4.0e10	100.04	0.975
0.02:0.06	8.0e9	4.0e10	59.12	0.934	3.4e8	4.0e10	100.04	0.975
0.01:0.03	1.1e9	4.0e10	46.52	0.942	3.5e8	4.0e10	98.13	0.974

Looking at the rotational correlation time τ_c, we can display two major differences between Q-band and X-band measurements, which are also highlighted in the main text:

1. the significant increase at bulk concentration 1.5 mM : 4.5 mM and

2. the higher τ_c values by 0.05 mM : 0.15 mM and 0.02 mM : 0.06 mM.

The first deviation occurs, because of a simultaneous decrease in both axial rotational diffusion tensors $D_\perp$ and $D_\parallel$, implying stronger electrostatic interactions throughout the entire ion cloud state and the tendency to form anisotropic ionic clusters. The second deviation is based on a minor decay in the $D_\perp$ tensor, which indicates changes in the molar ratio of 1:3 between $\mathbf{1}^{4+}$ and $\mathbf{3}^{2-}$. Smaller molar ratios lead to disturbances inside the ionic cloud state that hinder the formation of highly defined globular *ionoids*. In addition to the values in Table S.8 and S.9, we present the X- and Q-band CW EPR spectra for $\mathbf{1}^{4+}{:}\mathbf{3}^{2-}$ at all seven bulk concentration in Fig. S.12 to support the discussed differences.

Table S.9: Summary of the simulated axial rotational diffusion tensor $D_\perp$ and $D_\parallel$ as well as the calculated rotational correlation time τ_c and anisotropy T for pure Fremy's salt and $\mathbf{1}^{4+}{:}\mathbf{3}^{2-}$ in DMSO:glycerol:water 50:43:7 (v/v/v) at Q-band frequencies while changing the bulk concentration

c-ratio	$\mathbf{3}^{2-}$				$\mathbf{1}^{4+}{:}\mathbf{3}^{2-}$			
mM:mM	$D_\perp$ / s^{-1}	$D_\parallel$ / s^{-1}	τ_c / ps	T	$D_\perp$ / s^{-1}	$D_\parallel$ / s^{-1}	τ_c / ps	T
1.5:4:5	1.2e9	2.8e10	48.60	0.882	1.7e8	6.2e9	295.63	0.922
0.5:1:5	1.0e9	2.0e10	61.40	0.863	4.0e8	8.2e9	152.24	0.867
0.2:0.6	9.0e8	4.0e10	52.28	0.935	4.5e8	9.2e9	135.45	0.866
0.1:0.3	9.2e8	4.0e10	51.52	0.934	4.5e8	9.5e9	134.01	0.870
0.05:0.15	9.2e8	4.0e10	51.52	0.934	2.8e8	9.2e9	185.84	0.914
0.02:0.06	9.2e8	4.0e10	51.52	0.934	2.8e8	9.5e9	183.87	0.917
0.01:0.03	9.2e8	4.0e10	51.52	0.934	3.2e8	9.5e9	168.21	0.905
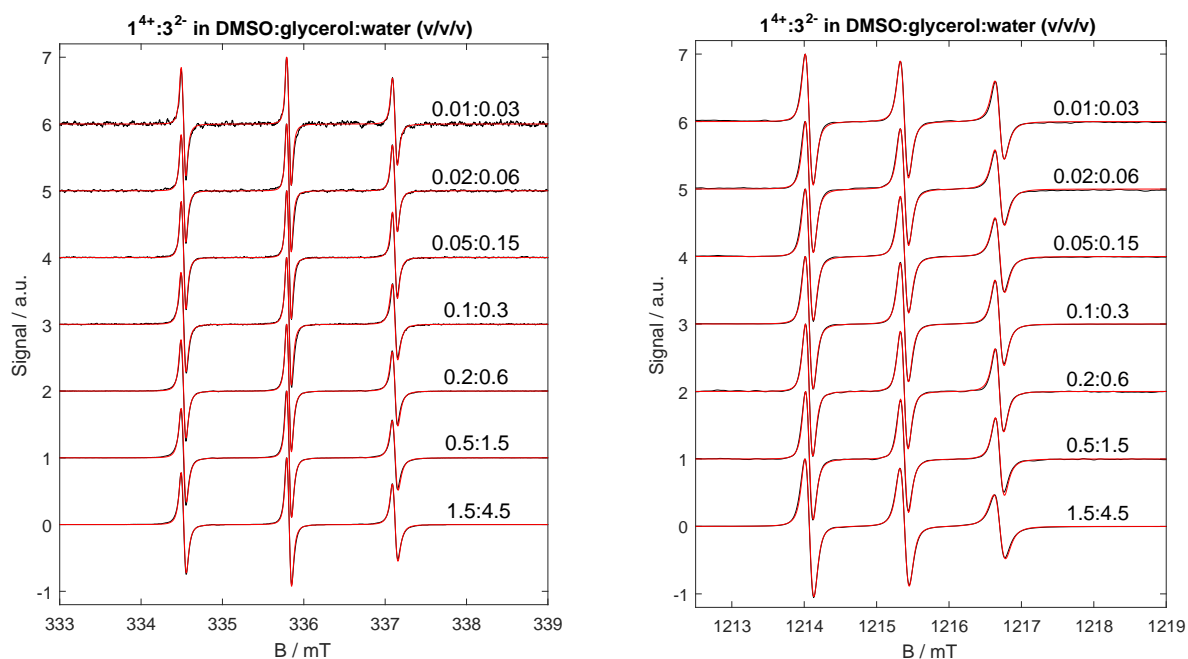
Fig. S.12: X-band (left) and Q-band (right) CW EPR spectra of $\mathbf{1}^{4+}{:}\mathbf{3}^{2-}$ in DMSO:glycerol:water 50:43:7 (v/v/v) with all seven bulk concentrations. The graphs again contain both the experimental data (black lines) as well as the simulated data (red lines).

Along with analysing the rotational correlation time τ_c for X- and Q-band, we focused on the full width at half maximum (FWHM) values of the simulated spectra, which are presented in Fig. S.13.
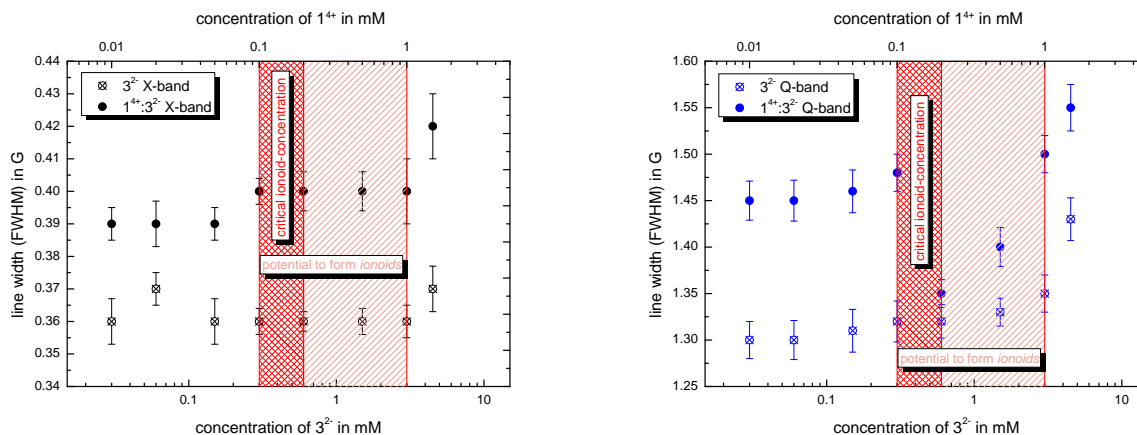
Fig. S.13: Isotropic broadenings of Fremy's salt and 1^{4+}:3^{2-} in DMSO:glycerol:water 50:43:7 (v/v/v) at different bulk concentrations for X-band (left) and Q-band (right) frequencies. Both graphs contain separated highlighted regions, which are based on the DLS data (see main text).

The X-band data represents a similar pattern like the rotational correlation time τ_c, which was discussed in the main text. Pure Fremy's salt displays no significant correlation between line width and concentration, while the system 1^{4+}:3^{2-} contains two 'steps':

1. between the highest bulk concentration 1.5 mM : 4.5 mM and the established 1 mM : 3 mM ratio and

2. after the 'critical *ionoid* concentration'.

The first drop in the FWHM line width indicates stronger electrostatic interactions between 1^{4+} and 3^{2-} at higher concentrations consistently inside the ion cloud state. Throughout the region, which is capable of forming *ionoids*, we get a constant line width, implying comparable global noncovalent interactions. Again we can not distinguish between globular *ionoids* and anisotropic ionic clusters like with DLS, because CW EPR just observes the inital ion cloud state. The second drop in the FWHM line width can be interpreted as a sign for reaching the 'critical *ionoid* concentration', but the difference compared to higher bulk concentrations is rather small.

Q-band CW EPR spectra deliver, just like the rotational correlation time τ_c, a different connection between FWHM values and bulk concentration. Pure Fremy's salt shows a prominent decreased line width while reducing the concentration from 4.5 mM to 3 mM probably due to less collisions between the paramagnetic molecules[10]. Adding 1^{4+} leads to i) an almost linear decay of the FWHM value between 1.5 mM : 4.5 mM and 0.2 mM : 0.6 mM and ii) a sudden increase in the line width at 0.1 mM : 0.3 mM, which then stays almost constant even for lower bulk concentrations. The first phenomena correlates with weaker electrostatic interactions between 1^{4+} and 3^{2-} and the possibility to

highlight the local environment of Fremy's salt due to higher frequencies/magnetic fields. The second effect, the sudden rise of the line width, can be interpreted with the formation of ion pairs between 3^{2-} and its K^+ counterions. In addition, we observe a similar 'jump' for the anisotropy T of the rotational diffusion tensor, which will be discussed in the next section.

Besides characterizing the rotational correlation time τ_c and FWHM values for both CW EPR frequencies, we also compare the behavior of the rotational anisotropy T (see Fig. S.14). The X-band spectra for pure Fremy's salt deliver a relatively constant anisotropy, which increases significantly while adding 1^{4+} due to present electrostatic interactions. Furthermore, we recognize slightly smaller T-values for bulk concentrations below the 'critical *ionoid* concentration', indicating weakend attractions between 1^{4+}:3^{2-} inside the ion cloud.
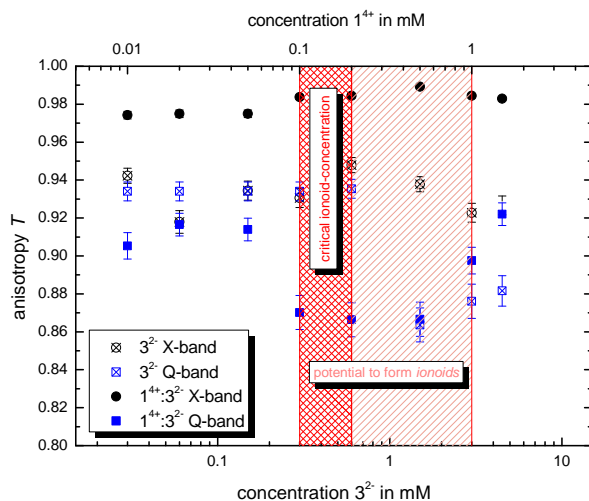
Fig. S.14: Plot of the anisotropy T of pure Fremy's salt and system 1^{4+}:3^{2-} in DMSO:glycerol:water 50:43:7 (v/v/v) for X- and Q-band against the concentration of 1^{4+} and 3^{2-}. The separated highlighted regions are based on the DLS results (see main text).

The anisotropy T based on the Q-band spectra display some major differences compared to the discussed X-band values. Pure Fremy's salt anisotropy decays slightly till 1.5 mM, but then rises to a constant value for all other concentrations. It seems 3^{2-} prefers the water phase inside the solvent mixture. At higher concentrations, Fremy's salt dissolves mainly in this more isotropic environment and thus reduces the anisotropy. Decreasing the concentration provides two possible reasons for the sudden jump in T:

1. the total number of 3^{2-} inside the water phase decays, which causes a reinforced signal from the nitroxide-ions in DMSO and glycerol or

2. the formation of ion pairs between 3^{2-} and K^+ inside the solvent.

The system $\mathbf{1}^{4+}$:$\mathbf{3}^{2-}$ also delivers a decay in T from $1.5\,\text{mM} : 4.5\,\text{mM}$ till $0.5\,\text{mM} : 1.5\,\text{mM}$, mainly due to weaker electrostatic forces between those two ions. In the region of the 'critical *ionoid* concentration', we do not see a change in the rotational dynamics, which indicates similar local attractions between $\mathbf{1}^{4+}$ and $\mathbf{3}^{2-}$ inside the ion cloud compared to the previous bulk concentration. Further decreases in the bulk concentration lead to higher T values, but here they do not surpass the results from pure Fremy's salt. We assume that $\mathbf{1}^{4+}$ prevents partially the formation of ion pairs of $\mathbf{3}^{2-}$ with K^+, leading to a comparatively isotropic environment.

References

1 S. W. Provencher, *Computer Physics Communications*, 1982, **27**, 213–227.

2 S. W. Provencher, *Computer Physics Communications*, 1982, **27**, 229–242.

3 Z. Li, Y. Wang, J. Schen and X. Sun, *Optics and Lasers in Engineering*, 204, **56**, 94–98.

4 M. Su, F. Xu, X. Cai, K. Ren and J. Shen, *China Particuology*, 2007, **5**, 295–299.

5 D. J. Schneider and J. H. Feed, in *Biological Magentic Resonance*, ed. L. J. Berliner and J. Reuben, Plenum Press, New York, 1989, ch. Calculating Slow Motional Magnetic Resonance Spectra, pp. 1–76.

6 S. Stoll and A. Schweiger, *Journal of Magnetic Resonance*, 2006, **178**, 42–55.

7 D. Hinderberger, *PhD thesis*, Johannes-Gutenberg-Universität Mainz, 2004.

8 D. Hinderberger and G. Jeschke, in *Site-specific Characterization of Structure and Dynamics of Complex Materials by EPR Spin Probes*, ed. G. A. Webb, Springer, 2006, ch. Characterization of Structure and Dynamics of Complex Materials, pp. 1529–1537.

9 D. Kurzbach, D. R. Kattnig, N. Pfaffenberger, W. Schärtl and D. Hinderberger, *ChemistryOpen*, 2012, **1**, 211–214.

10 B. H. Robinson, C. Mailer and A. W. Reese, *Journal of Magnetic Resonance*, 1999, **138**, 199–209.